Computation of Inviscid/Viscous Flowfield in Pulsed Lasers

B. Srivastava,* F. Faria-e-Maia,† and J. Moran*
Avco Research Laboratory, Everett, Massachusetts

This paper deals with two-dimensional flow and acoustic analysis in a pulsed laser system. The analysis method utilizes numerical solutions of the two-dimensional Euler/Navier-Stokes equations in the laser flow channel and one-dimensional Euler equations in the sidewall muffler volume with closely spaced baffles. Several comparative studies with experiments have been performed to establish the validity of the approach. Idealized laser-related problems have been computed to demonstrate the influence of sidewall muffler parameters on the transverse wave decay process in a laser cavity. An assessment of viscous effects on the cavity flow and acoustic clearing is also presented.

Nomenclature

a = nondimensional acoustic speed
e = nondimensional specific internal energy
$K_{m\ell}$ = normalized linear resistance in muffler backing volume, $K_{m\ell} L/\rho_r u_r$
K_{mn} = normalized nonlinear resistance in muffler backing volume, $K_{mn} L$
K_r = normalized linear resistance of muffler wall, $K_r/\rho_r u_r$
L = reference length
m = mass flux per unit area through the muffler wall orifice
M = Mach number
p = nondimensional pressure
Pr = Prandtl number (= 0.7)
Pr_t = turbulent Prandtl number (= 0.9)
R_h = wall roughness height normalized with L
Re_r = reference Reynolds number, $\rho_r u_r L/\mu_r$
t = nondimensional time
T = nondimensional temperature
u = nondimensional x component of velocity
u_e = inviscid core velocity
u_r = reference velocity, a_0
v = nondimensional y component of velocity
x,y = dimensionless Cartesian coordinates
$\bar{y}$ = nondimensional normal distance from the wall
ℓ = nondimensional length scale
α = open area ratio of the muffler wall
γ = ratio of specific heats
δ = boundary-layer thickness
ϵ = nondimensional eddy viscosity coefficient
μ = nondimensional first coefficient of viscosity
μ_r = reference viscosity coefficient, μ_0
ρ = nondimensional density
ρ_r = reference density, ρ_0
ω = vorticity

Subscript

0 = stagnation condition
t = partial derivative with time
w = wall values
y = partial derivative with y coordinate

Presented as Paper 87-1453 at the AIAA 19th Fluid Dynamics, Plasma Dynamics, and Lasers Conference, June 8–10, 1987; received Aug. 20, 1987; revision received March 29, 1988. Copyright © American Institute of Aeronautics and Astronautics, Inc., 1988. All rights reserved.

*Principal Research Scientist. Member AIAA.
†Research Associate.

I. Introduction

In a high rep rate pulsed laser cavity, necessary requirements for obtaining a laser beam of high optical quality are good baseflow medium homogeneity, efficient removal of waste heat, and effective damping of acoustic disturbances during the interpulse time. Baseflow medium homogeneity requirement issues are generally addressed through careful design of various flow control elements such as flow mixer, flow straightener, turbulence manipulator, contraction, and diffuser.[1,2] This paper does not address the baseflow medium homogeneity issue. Rep-pulsed acoustic issues are typically addressed through properly designed acoustic damping elements such as finite-capacity sidewall mufflers and flow-through absorbers. Critical flow design evaluations can be made using computational techniques that include appropriate modeling of such flow elements. Several past technical efforts[1-6] in this area suggest the utility of these predictive approaches. This paper deals with rep-pulsed acoustic issues.

In general, most of the predictive methods mentioned have been restricted to one-dimensional computational approaches. Progress to address transverse wave issues using two-dimensional computational approaches has been limited[7,8] due to the complexity of the problem involved. More work in developing two-dimensional inviscid computational approaches promises much desired predictive tools for laser applications. Furthermore, a recent survey[9] of the state-of-the-art in laser fluid dynamics has identified the need to develop viscous models to enhance further understanding of the complex flow phenomena in the laser cavity. Several viscous laser cavity transient flow phenomena such as boundary-layer growth, its interaction with the laser initiated acoustic pulse, the effect of muffler inflow/outflow on the channel flow, and the extent of flow reversal (if any) due to the acoustic pulse might play an important role in dictating a rational laser system design approach for optimum laser performance. An understanding of these flow phenomena is important for component system design. A validated two-dimensional viscous unsteady flow code with all the essential flow ingredients as previously outlined will be a useful analytic tool for predicting such flow phenomena.

This paper deals with two major technical issues related to the laser cavity acoustic clearing process. The first part deals with the impact of various design parameters on the transverse acoustic wave clearing process in an inviscid sense. To date this is an issue that has not been fully addressed using a physically complete flow model. This is accomplished in this paper by developing numerical solutions of the complete Euler equations in the laser cavity as well as in the muffler backing volume. This approach is distinctly different and physically more realistic than prior efforts in this area,[2-6] where muffler

backing volumes were treated in an approximate fashion. The second part of this paper deals with the impact of viscous effects on the laser cavity clearing process. The degree to which such effects may be important has not been previously explored. In this paper we have developed viscous models to assess these effects. The viscous model is based on the solution of turbulent Navier-Stokes equations in the laser flow channel.

This paper is divided into five sections. Section II describes the physical problem and the relevant theoretical model. Section III details the code validation tests and their results in an effort to establish a validated baseline code. Section IV describes several numerical studies aimed at developing an understanding of critical design issues related to two-dimensional and viscous effects. Finally, Sec. V summarizes the relevant conclusions.

II. Physical Problem and Theoretical Model

It is highly relevant to first understand the physics of the problem at hand. Figure 1 shows a typical near-cavity laser flow system consisting of a cavity of length L preceded by a sidewall muffler of length L_1, depth h_1 and followed by a muffler of length L_2, depth h_2. It is sufficient to consider near-cavity components since these components control the dominant acoustic damping processes. Also shown in the figure are typical representative longitudinal and transverse electron beam energy deposition profiles, which contribute to longitudinal and transverse acoustic waves, respectively. In some cases, a muffler placed directly above the laser cavity is used for rapid attenuation of the transverse waves.

The theoretical model for the previously outlined problem consists of solving the Euler/Navier-Stokes equations in the main flow channel. These equations are solved in a generalized coordinate system. For turbulent flow computations, the Baldwin-Lomax turbulence model is employed. The effects of wall roughness and suction/blowing are included in the appropriate turbulent length and velocity scales, as discussed by Van Driest[10] and Cebeci.[11] The complete channel equations written in body-fitted coordinates are discussed in Refs. 12 and 13. We discuss here only the relevant turbulence modeling method.

This model is a two-layer algebraic eddy viscosity model in which ϵ is given by

$$\begin{aligned} \epsilon &= \epsilon_i \qquad \bar{y} \le \bar{y}_c \\ &= \epsilon_o \qquad \bar{y}_c < \bar{y} \end{aligned} \tag{1}$$

where y is the normal distance from the wall and y_c is the smallest value of y at which values from the inner and outer formulas are equal. The Prandtl-Van Driest formulation in nondimensional form is used in the inner region:

$$\epsilon_i = Re_r \, \rho \, \ell \, |\omega| \tag{2}$$

where

$$\ell = k \, \bar{y} \, \{1 - \exp(-\bar{y}^+ / A^+) + \exp(-60 \, \bar{y}^+ / A^+ \, K^+)\}$$

$$\bar{y}^+ = \bar{y} \sqrt{Re_r \, \rho_w \, \tau_w / \mu_w}$$

$$A^+ = A^* \, e^{-5.9 \, v_w^+}$$

$$K^+ = R_h \sqrt{Re_r \, \rho_w \, \tau_w / \mu_w}$$

$$v_w^+ = v_w / \sqrt{\tau_w / \rho_w}$$

In the preceding expression, ω is the magnitude of the vorticity, and τ_w is the magnitude of the shear stress at the wall.

In the outer region the classical Clauser formulation[11] is replaced by the following model:

$$\epsilon_o = Re_r [K \, C_{cp} \, \rho \, F_w \, F_k(y)] \tag{3}$$

where K is the Clauser constant and C_{cp} is an additional constant. Furthermore,

$$F_w = \bar{y}_{\max} \, F_{\max}$$

The quantities $\bar{y}_{\max}$ and $F_{\max}$ are determined from the function

$$F = \bar{y} \, |\omega| \, [1 - \exp(-\bar{y}^+ / A^+)]$$

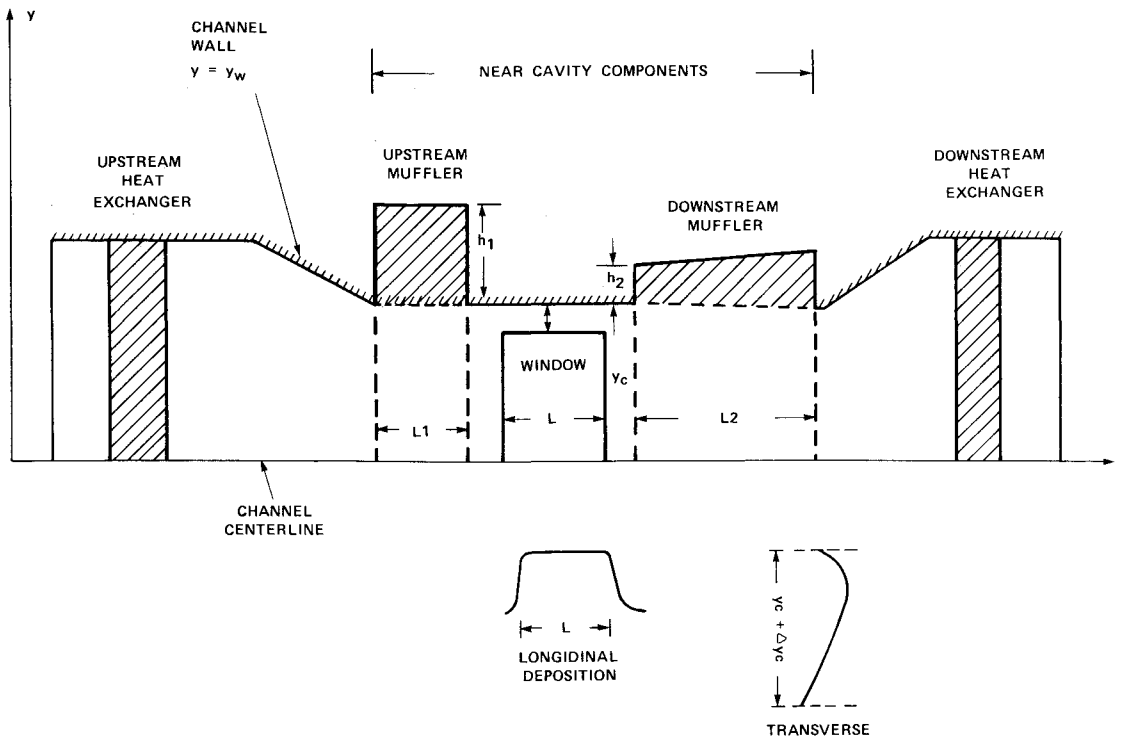

Fig. 1 Components of a typical pulsed laser system.

The quantity F_{max} is the maximum value of F that occurs in a profile, and $\bar{y}_{max}$ is the value of $\bar{y}$ at which it occurs. The function F_k is the Klebanoff intermittency factor given by

$$F_k(y) = [1 + 5.5(C_k\, \bar{y}/\bar{y}_{max})^6]^{-1}$$

The various standard constants appearing in the preceding equations are $k = 0.4$, $A^* = 26$, $K = 0.0168$, $C_k = 0.3$, and $C_{cp} = 1.6$.

The two constants introduced by Baldwin and Lomax, C_k and C_{cp}, can take different values for different flow speeds. Typical values are $C_{cp} = 1.6$ and $C_k = 0.3$ for equilibrium boundary layers at transonic speeds,[14] $C_{cp} = 1.2$ and $C_k = 0.65$ for an equilibrium incompressible boundary layer.[14] For applications to all turbulent flow problems here, the values of constants chosen were $C_{cp} = 1.2$ and $C_k = 0.65$.

The muffler model is based on the solution of unsteady one-dimensional Euler equations with source terms. These source terms represent linear and nonlinear loss terms typical of a porous material.[15] These equations are also solved in a generalized coordinate system to allow for variable muffler depth in a computational procedure. In a rectangular coordinate system, these equations are written as (see Fig. 1)

$$\rho_t + (\rho v)_y = 0 \tag{4a}$$

$$\rho\, v_t + \rho v\, v_y + p_y = -D_y \tag{4b}$$

$$\rho\, e_t + \rho v\, e_y + p\, v_y = 0 \tag{4c}$$

$$p = (\gamma - 1)\, \rho e \tag{4d}$$

$$D_y = K_{m\ell}\, v + K_{mn}\, \rho\, |v|\, v \tag{4e}$$

These equations are written in a nondimensional form. Here, $K_{m\ell}$ and K_{mn} are dimensionless coefficients representing linear and nonlinear losses in the backing volume. The assumption of zero axial velocity in the muffler backing volume is physically realistic and is consistent with the closely spaced baffle approximation.[3] This muffler model is an improvement over prior efforts[3-6] that did not include the effects of muffler depth in the computational effort. Acoustic reverberations in the sidewall muffler would be important if the muffler depth were not very small compared to the channel height.

Muffler walls are treated by a quasisteady model for flow-through orifices.[3-6] These equations are

$$m = \alpha\, \rho_h\, v_h \tag{5}$$

Outflow:

$$M_h = \min\left\{\left[\frac{2}{\gamma - 1}\left(\frac{p_c}{p_m}\right)^{(\gamma-1)\gamma} - 1\right]^{1/2}, 1\right\} \tag{6a}$$

$$\rho_h\, v_h = C_d \frac{\gamma\, p_c\, M_h}{a_c\left(1 + \dfrac{\gamma - 1}{2} M_h^2\right)^{(\gamma+1)/2(\gamma-1)}} \tag{6b}$$

Inflow:

$$M_h = \min\left\{\left[\frac{2}{\gamma - 1}\left(\frac{p_m}{p_c}\right)^{(\gamma-1)/\gamma} - 1\right]^{1/2}, 1\right\} \tag{7a}$$

$$\rho_h\, v_h = C_d \frac{\gamma\, p_m\, M_h}{a_m\left(1 + \dfrac{\gamma - 1}{2} M_h^2\right)^{(\gamma+1)/2(\gamma-1)}} \tag{7b}$$

where C_d is the discharge coefficient (~ 0.6). Subscript c refers to the channel side of the perforated wall, m refers to the muffler side of the wall, and h denotes the properties in the hole. A thin porous mat placed over the perforated plate separating the channel and the muffler can be simulated by replacing p_c by $p_c + k_r\, v_h$ in the above equations. Here, the coefficient k_r is utilized to characterize a linear loss term in the wall perforations.

It can be shown that for small Δp, Eq. (5) may be reduced to the appropriate loss form (follows from a series expansion for low Δp)

$$\Delta p \sim \rho_h\, |v_h|\, v_h / 2\, C_d + k_r\, v_h \tag{8}$$

Thus, the muffler wall typically is characterized by a linear and nonlinear loss term. In the determination of discharge coefficient C_d, the grazing flow effects have been included. Asymptotic values of the boundary conditions of Eqs. (5-7) are used for small Δp to avoid numerical errors.

The transport of momentum and energy for outflow/inflow follows from quasisteady flow-through orifices. For details of this, the reader is referred to Ref. 3 where all relevant equations are described.

An explicit time-marching MacCormack predictor-corrector scheme is employed for all computations. A typical numerical procedure consists of time-advancing the channel and backing volume equations while all boundary conditions are imposed explicitly at the end of both predictor and corrector steps. For channel equations an unsplit cell-centered MacCormack scheme is used.

III. Comparison with Experiments

The turbulent two-dimensional viscous/inviscid, steady/unsteady problems in the laser flow are complex in nature. Perhaps the most complex turbulent viscous flow phenomena are the interaction of the base flow turbulent boundary layer with the laser initiated shocks/expansions and the associated thermal interfaces. These flow phenomena are characterized by transient shock/expansion-boundary-layer interactions, pressure-wave-induced muffler suction/blowing, and wall roughness effects due to muffler material and wave interactions with porous material. We have attempted to validate the present computational approach by selecting appropriate available data either from literature or from inhouse experiments. Several of these validation tests have been based on steady flow measurements characterizing a typical flow process encountered in a transient laser environment. Lacking further test data, these validation tests are considered adequate. A large number of such steady-state validation tests have been reported before, using this baseline code.[12,13,16] Further code validation test results are presented here.

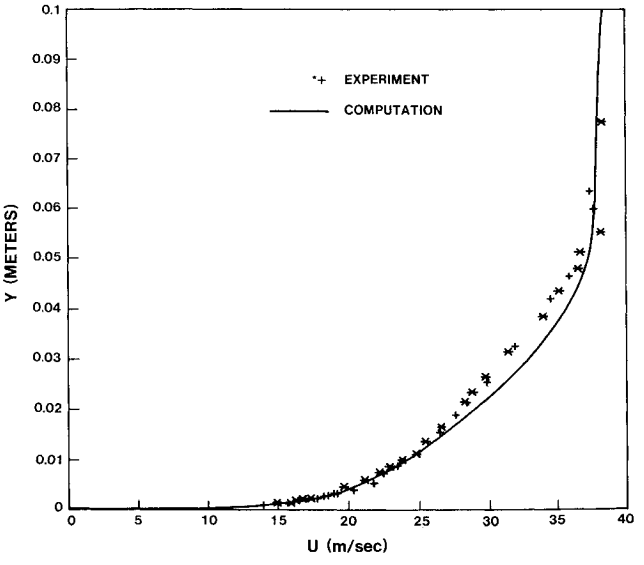

Fig. 2 Comparison of computed velocity profile with experimental data for a rough wall; $M_\infty = 0.1$, $Re_\infty = 5.4 \times 10^6$, 73.6 mil roughness height.

To characterize the effects of roughness in the viscous code, the experimental configuration of Blake[17] was simulated. This experiment was conducted on a flat plate at a flow Mach number of 0.1, Reynolds number of 5.4×10^6 (based on $L = 88$ in. where profile measurements were taken), and a roughness height of 73.6 mil (0.0736 in.). Figure 2 shows a good overall comparison of the computed results and the corresponding experimental data.

To characterize the effects of suction and blowing in the viscous code, the experiments of Avidor[18] and Simpson[19] were selected for simulation. Figure 3 shows computational results and the corresponding experimental data of Avidor.[18] These suction experiments were conducted at flow Mach numbers of 0.1 and 0.2. We have simulated the suction experiments at a flow Mach number of 0.1. For this experiment, the Reynolds number based on 30 cms (where profile measurements were taken) was 9×10^5. We have simulated these experiments at suction velocities of 0.25 and 0.5% of core velocity. Figure 3 shows the predicted boundary-layer thickness as compared to the experiments for the no-suction case and for the two-suction velocities previously mentioned. The comparison between the predicted results and experimental data is reasonably good. In an effort to compare the predicted velocity profile with suction experiments, we selected the test data of Simpson (where some detailed measurements were made). This experiment was conducted at a Mach number of 0.04 and Reynolds number of 9.3×10^5 (based on 42 in. length where profile measurements were made). The suction velocity for this case was 0.24% of core velocity. Figure 4 shows a fairly good comparison of the computed and measured profile. Figure 5 shows the computed result for a blowing case corresponding to the test data of Simpson.[19] Here, the Mach number was 0.04 and Reynolds number $\sim 4.0 \times 10^5$ (based on 18-in. length where profile measurement was taken). The blowing rate for this case was 0.4% of core velocity. It is apparent from this figure that the comparison between predicted results and experiments is very good.

An important and relevant code validation test relates to the response of a porous material for an input wave typically encountered in laser applications. We have conducted a code validation test using a square wave input on a porous material [characterized by linear and nonlinear losses; see Eqs. (4)]. The results have been compared with a recent shock-tube experiment.[20] Figures 6a and 6b show the results obtained from the inviscid code as compared to the experimental result. In Fig. 6a, the results are presented in terms of attenuation of the square pulse ($\Delta p_x/\Delta p_i$) vs distance traveled through the porous material. Details of the porous material characteristics are also shown in Fig. 6a. These were obtained from pressure-drop measurements of the porous material. The comparison between the predicted results and the experimental measurement is reasonably good for both zero-flow Mach number and at a flow Mach number of $M = 0.026$. Higher pulse decay rate at a finite-flow Mach number is due to the increased flow resistance of the porous material as the flow Mach number is increased. Figure 6b shows a comparison of the computed inlet and exit pressure variation with time for the porous plug as compared to the experimental measurements. The magnitude of the reflected and transmitted pulses through the porous material as well as their temporal variations compares very well with experimental measurements.

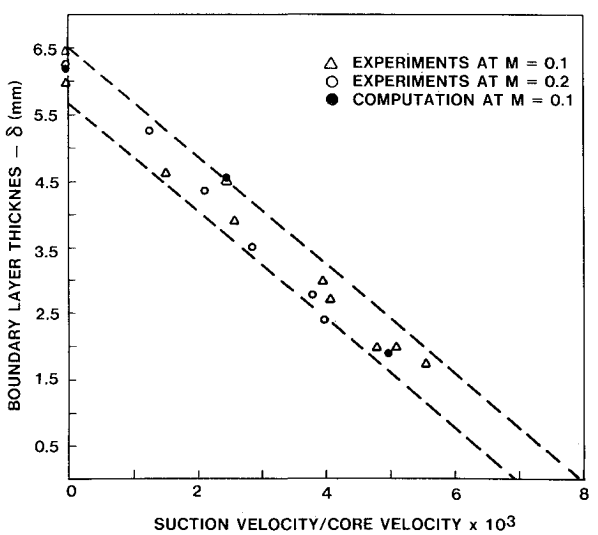

Fig. 3 Comparison of computed boundary-layer thickness with experimental data for various suction velocities; $M_\infty = 0.1$, $Re_\infty = 9 \times 10^5$.

IV. Laser-Related Acoustic Studies

The prime motivation (and therefore utility of the code described) of this paper is to develop an understanding of the controlling design parameters that can effectively damp transverse waves in a laser cavity during an interpulse time. In this section, we discuss specific studies demonstrating the utility of such a design tool for single-pulse computations.

It is prudent to discuss some numerical results to show how this computation can help develop insight into design considerations for a laser system. For illustration, an isolated muffler parametric study is shown. The two-dimensional inviscid unsteady code was used for this study. Figure 7 shows a sketch of the laser cavity and muffler arrangement with controlling nondimensional design parameters. The muffler

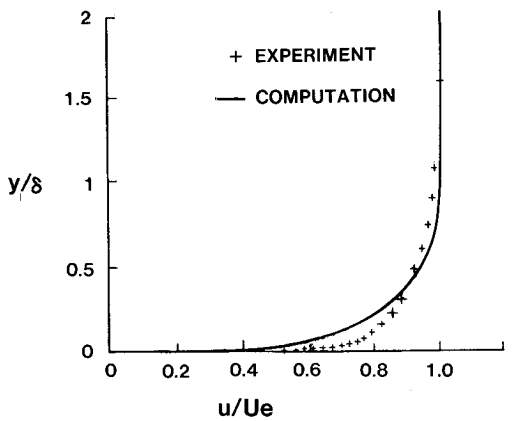

Fig. 4 Comparison of computed velocity profile with experimental data with wall suction; $M_\infty = 0.04$, $Re_\infty = 9.3 \times 10^5$, $v_w/u_e = -0.0024$.

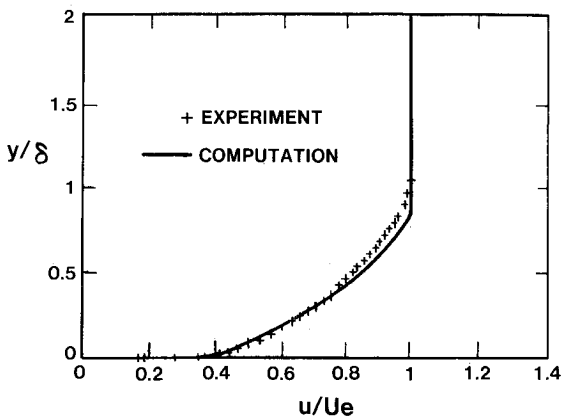

Fig. 5 Comparison of computed velocity profile with experimental data with wall blowing; $M_\infty = 0.04$, $Re_\infty = 4.0 \times 10^5$, $v_w/u_e = 0.004$.

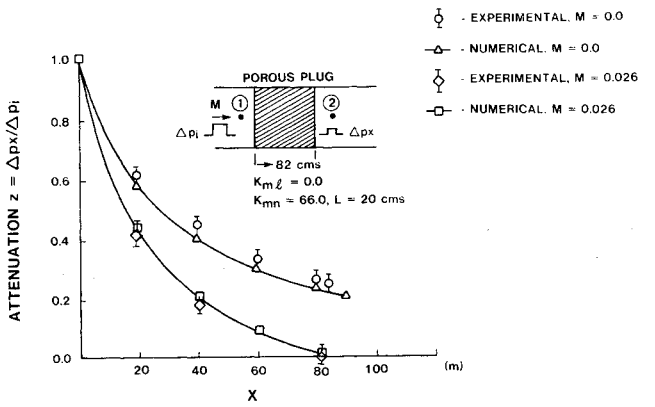

Fig. 6a Comparison of computations and experimental data for the attenuation of an input pulse through a porous plug; shows attenuation of the leading edge of the input wave.

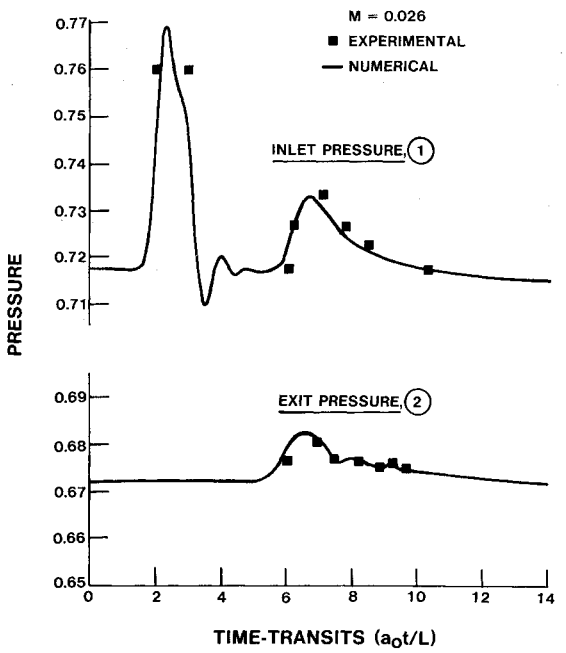

Fig. 6b Comparison of computations and experimental data showing response of the porous plug shown in Fig. 6a; inlet and exit pressures are shown for $M_\infty = 0.026$.

wall linear resistance is K_r, the open area ratio of the muffler is α, the discharge coefficient is C_d, the muffler backing depth linear resistance is K_{mt}, and the backing depth nonlinear resistance is K_{mn}. Figures 8 and 9 show predictions of cavity root mean square pressure perturbations clearing with time normalized by sound speed and cavity height H for various values of the muffler parameters.

Two cases are shown here. Figures 8a–8c show the situation when the transverse energy deposition is uniform. The uncorrected curves in these figures relate to root mean square cavity pressure perturbations with piston term removed, while the linear correction relates to the same with a linear term removed. For laser application, the first implies medium perturbations over the instantaneous average value, while the second relates to medium perturbations after an instantaneous tilt term correction through cavity mirrors. In this case, uniform overpressure in the cavity causes a transverse wave whose strength is primarily controlled by the muffler wall resistance. In the absence of a cavity muffler (i.e., infinite wall resistance). the overpressure in the cavity causes only longitudinal waves, which are expected to clear the cavity in nearly

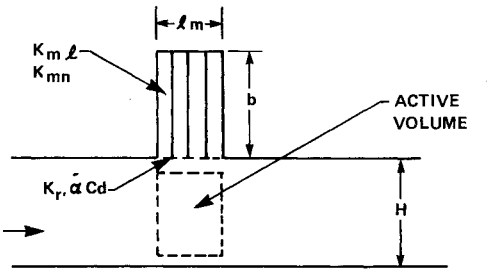

Fig. 7 Schematic showing a muffler placed over the active laser cavity for acoustic damping; basic nondimensional design parameters are $\ell m/H$, b/H, K_{mt}, K_r, and αC_d.

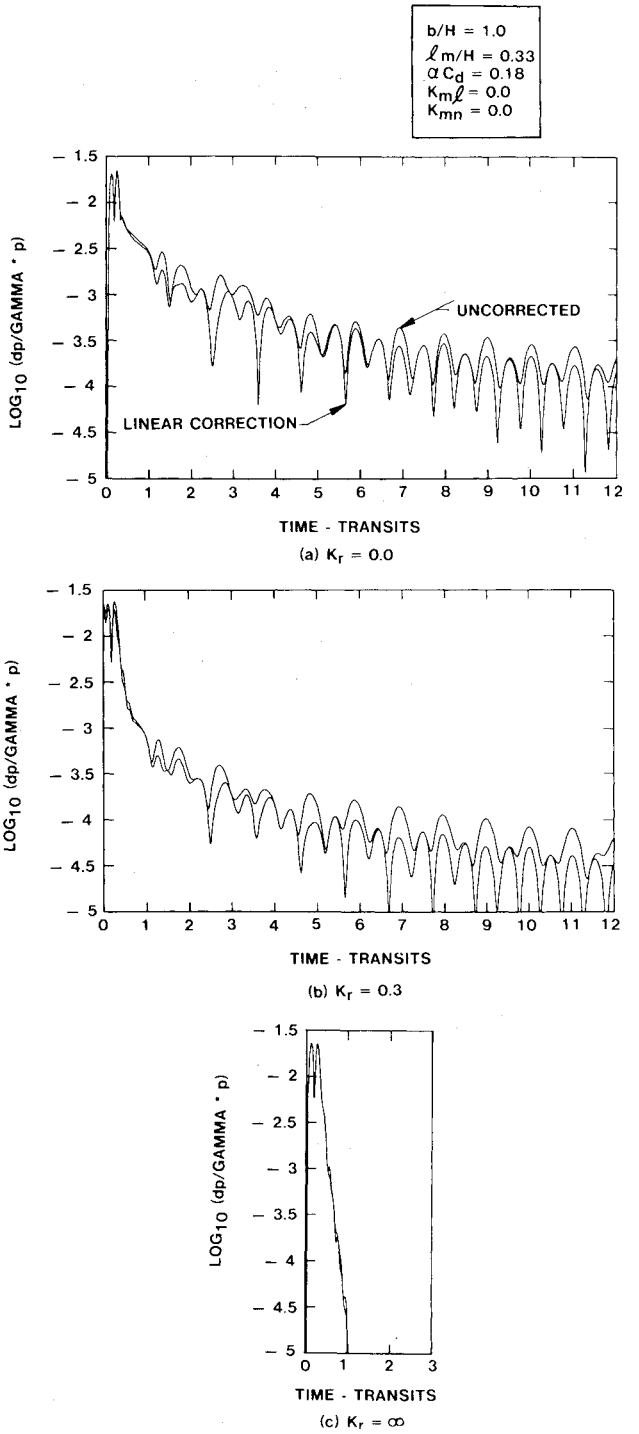

Fig. 8 Computations showing the influence of muffler wall resistance on the clearing of pressure perturbations in the laser cavity with uniform deposition in transverse direction.

one acoustic transit. However, the presence of cavity muffler with finite muffler wall resistance causes transverse expansion, resulting in the generation of transverse waves. Figure 8a shows the nature of the transverse wave when the wall resistance $K_r = 0.0$. Figure 8b shows the nature of the same transverse wave when $K_r = 0.3$. As one would expect, the strength of the transverse wave for the latter case is less than the former. These results can be compared with Fig. 8c when muffler wall resistance is infinite (i.e., the hardwall case). It is of interest to note that, in Figs. 8a and 8b, the early time (i.e., less than one transit) wave phenomena is dominated by longitudinal wave clearing, whereas later (greater than one transit), the cavity is dominated by the transverse wave effects. The latter, however. decays very slowly. This is reflected in the change of slope for the wave clearing process. From these results it is clear that cavity muffler would be harmful in cases where no significant energy deposition nonuniformity exists in the transverse direction. In most practical applications, however, this is not so. Thus, we must analyze situations where substantial transverse nonuniformity in energy deposition exists. Only in such cases one can demonstrate the benefit of using a sidewall cavity muffler. Figure 1 shows the deposition profile that we have used for the computations outlined next.

Figures 9a–9c show a series of calculations where the linear backing depth resistance was gradually increased to assess the influence of this parameter on the transverse wave decay rate. The various curves in these figures have the same meaning as in Fig. 8. However, we have also presented here the cavity root mean square pressure perturbations with a quadratic term removed. This relates to instantaneous focus correction through cavity mirrors. Figure 9a shows the decay behavior when the linear resistance $K_{m\ell}$ in the backing depth was taken to be zero. The cavity clearing process is clearly dominated by strong transverse wave reverberations. Figures 9b and 9c show corresponding results when the value of $K_{m\ell}$ was increased to 0.2 and 1.0, respectively. The decay behavior is clearly altered. It appears, however, that there is an optimum linear muffler backing depth resistance beyond which the gain in transverse wave clearing is marginal. These observations and decay behavior are qualitatively similar to what has been determined in a recent controlled shock-tube experiment.[20]

An interesting physical picture emerges, however, if one looks at the details of the pressure variation in the muffler and the laser cavity for the computation shown in Figs. 9a and 9c. Figure 10 shows such a result. This figure shows pressure variations near the muffler wall on the two sides of the muffler wall for two different muffler linear resistance parameters (Resistance parameters are normalized with freestream value ρa, where ρ is the density and a is the acoustic speed.) Notice that at a large value of $K_{m\ell} = 1.0$ (as compared to Fig. 10a with $K_{m\ell} = 0.0$), as in Fig. 10b, the muffler first behaves like a solid wall (due to high induced transverse velocity causing the resistance to flow to be very high). At a later time, ~ 0.6 transits, when initial waves have subsided, the muffler becomes soft, and a damped acoustic wave pattern is established. Notice from comparison that the wave pattern and its decay is significantly different for the two values of $K_{m\ell}$, indicating the usefulness of such predictive tools in assessing the influence of various parameters on the overall design.

Based on these results, a design strategy for transverse wave control can be formulated. Three competing effects must be considered for choosing a wall muffler in the laser cavity. These are bulk overpressure generated transverse waves, transverse waves due to the cavity loading nonuniformity, and the outflow of hot gas from the muffler backing volume at late times. The last of these could be of severe consequence if not confined within the wall boundary layer (which is excluded from the cavity active volume) from a laser beam quality standpoint. Sometimes even if confined within the wall boundary layer, it may not be acceptable due to its impact on cavity electrodynamics. Thus, a choice of cavity muffler must

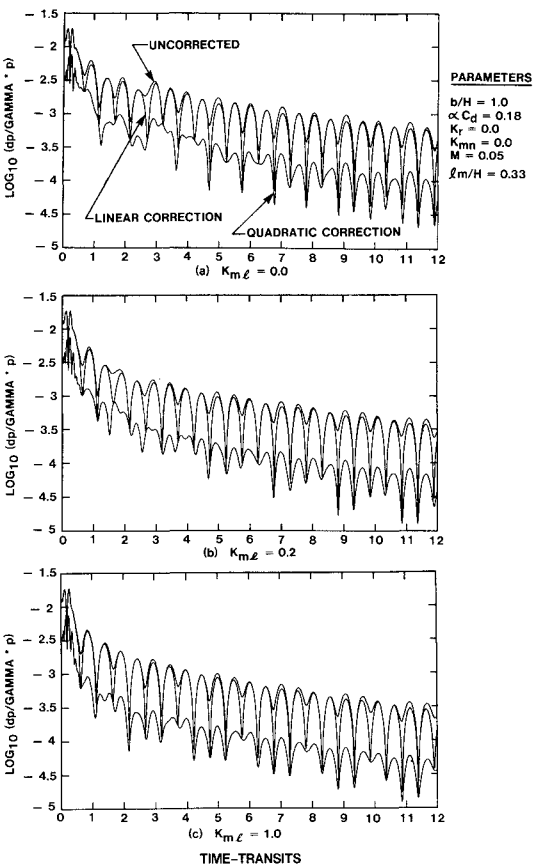

Fig. 9 Computations showing the influence of linear resistance in the backing volume of the muffler on the clearing of pressure perturbations in the laser cavity with nonuniform transverse deposition.

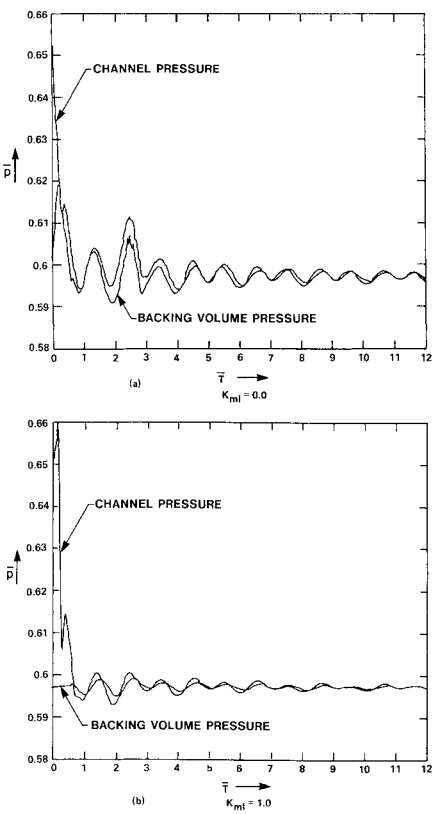

Fig. 10 Computed pressure at cavity side of the muffler wall and muffler side of the muffler wall showing the transient behavior of acoustic waves for the case shown in Fig. 9.

be carefully weighed from these three considerations. In general, the transverse wave due to nonuniform cavity loading is only a few percent of the cavity overpressure. A typical cavity acoustics decay process is, therefore, first dominated by longitudinal clearing (a more rapid process) and then later a slower transverse clearing process (see Figs. 9a–9c). The design strategy should be based on changing the acoustics decay rate at late times (i.e., greater than 2–3 transit times as in Fig. 9). This can be done by choosing cavity wall muffler and backing depth resistance such that the muffler remains acoustically stiff at early times (when cavity pressures are very high) and thus not allowing any substantial amount of hot gas to penetrate muffler backing volume during this time. This strategy also prevents generation of strong transverse waves due to the initial large cavity overpressure. At late times, the wall muffler resistance decreases (a transient effect since the wall resistance is proportional to the induced velocity caused by the transverse waves), leading to the wave and hot gas penetration into the muffler volume. The amount of hot gas injected into the backing volume, however, will be substantially smaller using this strategy. Whether it is possible to select muffler parameters to achieve this or not is demonstrated in Figs. lla and llb, where muffler parameters were first selected to make the wall muffler acoustically stiff, as in Fig. 11a, and then were readjusted to relieve this stiffness, as in Fig. 11b. The evolution of this philosophy is attributable to the studies shown in Figs. 8–10. This design strategy is being used currently in most of our laser applications where a cavity muffler is necessary for damping transverse waves.

Viscous effects can influence the predicted results outlined, even though boundary layers near the cavity sidewalls are typically excluded from the active cavity laser volume. The basic physical mechanisms are through generation of additional waves by the shock-boundary-layer interaction process, suction/blowing mechanisms of boundary layer through sidewall muffler, and possible flow reversal of the low-momentum flow near the wall. The primary issue is whether any of these effects alter the basic cavity clearing predicted by inviscid models.

We have conducted a transient viscous simulation to understand the early time behavior for a problem by incorporating viscous turbulent effects. A typical problem that was chosen consisted of base flow Mach number of 0.055, $b/H = 0.5$, and $Re \simeq 10^6$ (based on cavity height H). For assessing viscous effects, it is not necessary to perform a complete calculation during the interpulse time, since such effects, if significant, will show up in our early time computations. For upstream and downstream propagating waves, the wave boundary-layer interactions would result in additional waves that travel with acoustic speed. Thus, these effects should show up in early time computations. For acoustic waves moving into the backing volume, through boundary layers near the wall, an appropriate time scale is two times the acoustic transit time through the depth of the backing volume. Thus, all viscous-related effects can be observed in an early time transient simulation. There is, however, one exception to this. Particle motion within the backing volume is expected to be small, and its effect in the main cavity channel can show up much later in time as entropy disturbances. This, however, is not of interest in current studies, since any leakage of such a flow is primarily confined within the boundary layer. This happens due to very low momentum associated with such a leakage. Thus, our viscous simulations are confined to about 2.0 acoustic transits based on cavity height H.

The problem shown in Fig. 7 for inviscid computation was recomputed by including turbulent boundary layers near cavity walls. This was done by first developing a steady-state

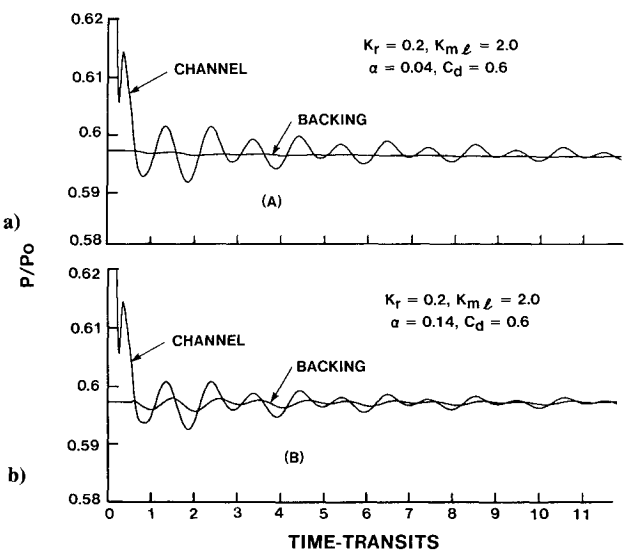

Fig. 11 Computations demonstrating control of cavity muffler response; a) acoustically stiff muffler, b) acoustically soft muffler.

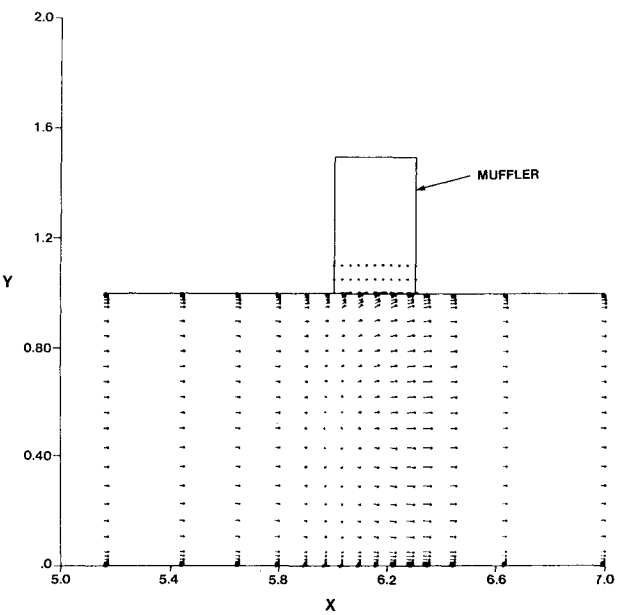

Fig. 12 Viscous flow computation showing early time flow pattern in the laser cavity; injection into the muffler, boundary layer flow reversal and transient wave effects are evident in this figure.

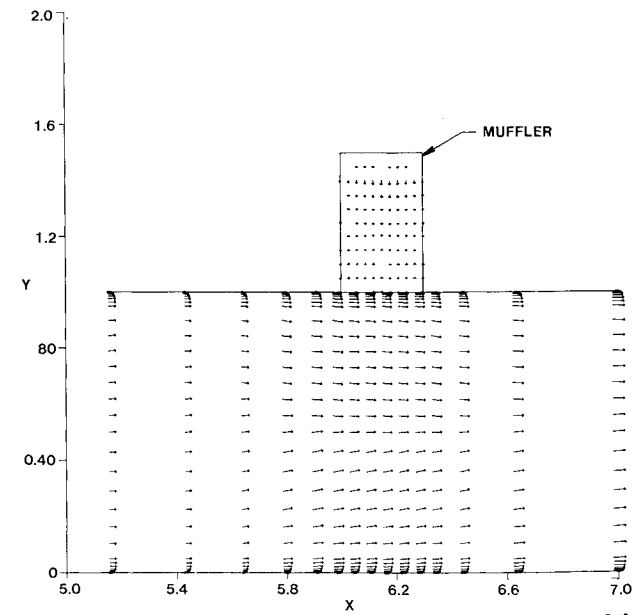

Fig. 13 Viscous flow computation at $t = 0.9$ showing recovery of the bulk flow in the active laser cavity; significant muffler reverberations; transverse wave in the main channel and near muffler boundary layer perturbations are evident.

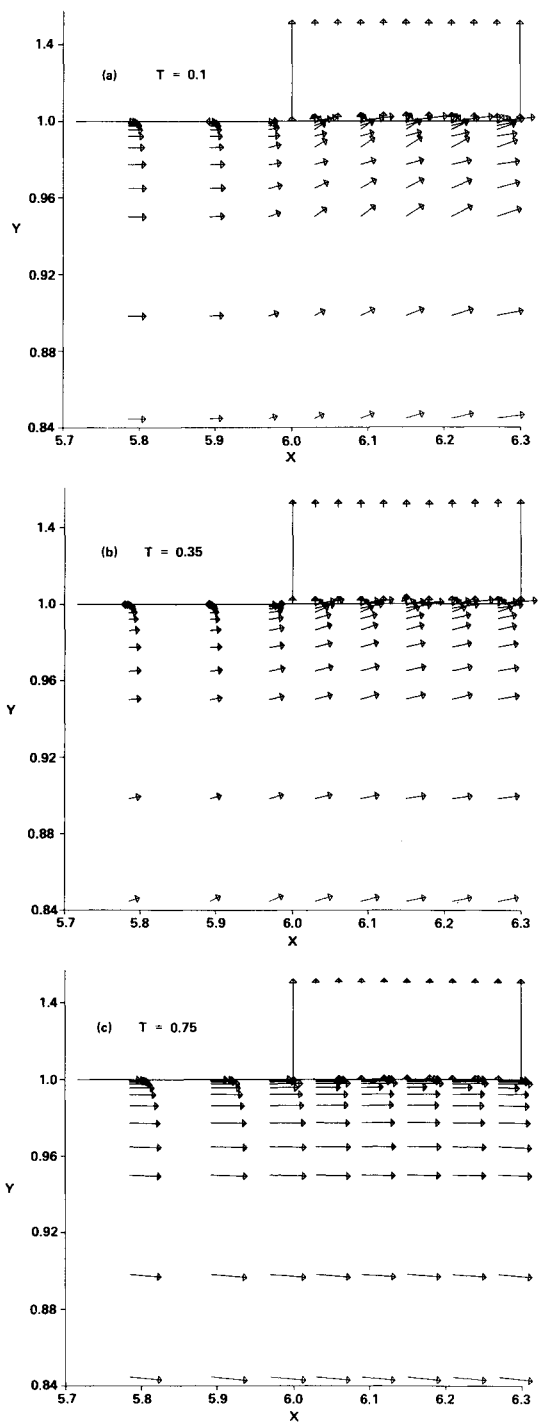

Fig. 14 Viscous flow behavior near the muffler wall for various times depicting complex early time characteristics.

turbulent viscous solution at an inlet Mach number of 0.055 and a Reynolds number of $\sim 10^6$ in the laser cavity. The unsteady turbulent viscous solution was then performed using this steady-state solution as the base flow. Figure 12 shows a typical flow pattern at an early time in the entire computational domain. Several interesting physical features are evident from this figure. Strong longitudinal and transverse waves have a dramatic effect on the flow pattern in the laser cavity. Typical physical processes that are seen in this figure are bulk flow reversal, complete suction of the boundary layer near the muffler wall, and flow penetration into the muffler. The primary question is whether any of these effects persist in time to have a detrimental effect on the laser cavity performance, either from a bulk flow behavior or acoustic behavior standpoint. We have attempted to answer this question by observing the development of the flow behavior with time. Figure 13 shows the cavity flow behavior at a later time $t \sim 1.0$. It is observed from this figure that the bulk flow behavior has improved due to longitudinal wave clearing from the cavity. This would imply that within a very short time (~ 1–2 acoustic transits), the bulk flow in the active laser cavity volume (excluding the near-wall boundary layer) essentially returns to the base flow state. A clearer picture emerges when one examines the near muffler domain in time. Figures 14a–14c show this result. Notice from Fig. 14a that at an acoustic transit time $t = 0.1$, the bulk flow has a dominant upward particle motion caused by the transverse waves in the cavity. The boundary layer near the upper wall is seen to be completely sucked by the flow injection into the backing volume. The particle velocity within the backing volume itself appears to be small compared to the main channel. Further continued injection is seen to increase the particle velocity in the backing volume as in Fig. 14b at $t = 0.35$. At a further later time at $t = 0.75$, the cavity particle velocity has a downward dominant motion caused by transverse waves within the cavity itself. At $t = 0.9$, as shown in Fig. 13, the cavity bulk flow is clear of any significant effect on the particle velocity except near the walls. Assessment of such effects is important for achieving high rep-rate high power output lasers.

We also have examined the details of the cavity acoustic clearing process for viscous simulation at early times in an effort to identify any significant differences from inviscid simulation. These findings suggest that pressure perturbations averaged (root mean square) over the active cavity volume (which excludes wall boundary layers) show a behavior similar to those observed in inviscid simulations. This conclusion is applicable primarily to the case that has been studied here. Our detailed analysis suggests that a combination of high Reynolds number (thin boundary layer), low cavity overpressure (weak wave strength), and strong transverse nonuniformity (dominant inviscid transverse clearing) results in a physical situation that is primarily dominated by inviscid phenomena.

V. Conclusions

This paper deals with the development of a validated two-dimensional inviscid/viscous, steady/unsteady computational procedure that can address critical flow and acoustics system design issues typical of a pulsed laser. The motivation for this generalized approach is attributed to the need to understand the decay of laser cavity transverse acoustics due to the specific choice of various acoustic suppression design parameters and near-wall viscous effects. This has been achieved here by developing numerical solutions of the Euler/turbulent Navier-Stokes equations in the laser flow channel and Euler equations in the muffler backing volume. Several code validation tests also have been performed to establish the validity of this computational procedure.

Computational studies have been performed by simulating idealized laser configurations in an effort to demonstrate that the laser generated cavity transverse wave decay process can be enhanced by an optimum choice of specific acoustic suppression design parameters. This optimum configuration selection yields improved cavity acoustic performance.

Computational studies also have been performed to assess the impact of viscous effects on the cavity flow recovery process. These studies suggest that even though the instantaneous flow pattern due to the laser initiated acoustic pulse is quite complex, the laser cavity bulk flow essentially returns to the base flow state within a short time. Analysis of viscous results suggests that for high Reynolds number flows with weak cavity waves and strong transverse nonuniformity, the inviscid acoustic clearing predictions are essentially unaltered.

Acknowledgment

The work reported in this paper was sponsored by Avco Research Laboratory (ARL) independent research and development funds. The authors are indebted to the ARL Ground Based Laser Program office for financial support in this area.

References

[1]Tong, K. O., Knight, C. J., Singh, P.I., and Srivastava, B. N., "Flow and Acoustics Study for Pulsed Visible Lasers," AIAA Paper 80-0348, Jan. 1980.

[2]Hurdle, M. P., Morris, M. J., Hogge, D. H., and Crow, C. S., "Flow and Acoustics in Pulsed Excimer Lasers – A Novel Design," AIAA Paper 79-1487, July 1979.

[3]Srivastava, B. N., Knight, C. J., and Zappa, O. L., "Acoustic Suppression in a Pulsed Laser System," *AIAA Journal*, Vol. 18, May 1980, pp. 555–562.

[4]Srivastava, B. N., "Pressure Wave Attenuation due to Anode Mufflers in Pulsed Lasers," *AIAA Journal*, Vol. 21, March 1983, pp. 381–389.

[5]Ausherman, O. R., Alber, I. E., and Baum, E., "Acoustic Suppression in a Pulsed Chemical Laser," *AIAA Journal*, Vol. 17, May 1979, pp. 490–497.

[6]Thayer, W. J., III., Buonadonna, V. R., and Cherman, W. D., "Pressure Wave Suppression for a Pulsed Chemical Laser," AIAA Paper 78-1216, July 1978.

[7]Knight, C. J., "Transverse Acoustic Waves in Pulsed Lasers," *AIAA Journal*, Vol. 20, July 1982, pp. 933–939.

[8]Kulkarny, V., "Decay of Transverse Acoustic Waves in a Pulsed Gas Laser," *AIAA Journal*, Nov. 1980, pp. 1336–1341.

[9]Cassady, P. E., "Fluid Dynamics in Closed Cycle Pulsed Lasers," *AIAA Journal*, Vol. 23, Dec. 1985, pp.1922–1931.

[10]Van Driest, E. R., "On Turbulent Flow near a Wall," *Journal of Aerospace Science*, Vol. 23, Nov. 1956, pp. 1007–1011.

[11]Cebeci, T., "Behavior of Turbulent Flow near a Porous Wall with Pressure Gradient," *AIAA Journal*, Vol. 8, Dec. 1970, pp. 2151–2156.

[12]Srivastava, B. N. and Bozzola, R., "Efficient and Accurate Numerical Solutions of the Euler and Navier-Stokes Equations for Turbomachinery Applications," AIAA Paper 84-1300, June 1984.

[13]Srivastava, B. N. and Bozzola, R., "Computation of Flowfields in High Turning Angle and High Solidity Cascades using Euler Equations," *Journal of Propulsion and Power*, Vol. 3, Jan. 1987, p. 39.

[14]Visbal, M. and Knight, D., "Evaluation of Baldwin-Lomax Turbulence Model for Two-Dimensional Shock Boundary Layer Interactions," AIAA Paper 83-1697, July 1983.

[15]Beavers, G. S. and Sparrow, E. M., "Compressible Gas Flow through a Porous Material," *International Journal of Heat and Mass Transfer*, Vol. 14, 1971, pp. 1855–1859.

[16]Srivastava, B. N., "Numerical Solution of the Euler Equations for Turbomachinery Applications, Part I Inviscid Test Problems, Part II Viscous Test Problems," Avco Everett Research Lab., Inc., Everett, MA, Final Rept., Feb. 1984.

[17]Blake, W. K., "Turbulent Boundary Layer Wall Pressure Fluctuations on Smooth and Rough Walls," Dept. of Naval Architecture and Marine Engineering, MIT, Cambridge, MA, Rept. 70208-1, Jan. 1969.

[18]Avidor, J., "Flow and Acoustics Study for Repetitively Pulsed Excimer Lasers," U.S. Army Missile Command, Redstone Arsenal, AL, Final Rept., April 1983.

[19]Simpson, R. L., "The Turbulent Boundary Layer on a Porous Plate; an Experimental Study of the Fluid Dynamics with Injection and Suction," Ph.D. Thesis, Stanford Univ., CA, 1968.

[20]Vu, B. T., "Shock-Tube Experiments," private communication, Avco Everett Research Lab., Inc. Everett, MA, Feb. 1987.

Recommended Reading from the AIAA Progress in Astronautics and Aeronautics Series . . .

MHD Energy Conversion: Physicotechnical Problems

V. A. Kirillin and A. E. Sheyndlin, editors

The magnetohydrodynamic (MHD) method of energy conversion increases the efficiency of nuclear, solar, geothermal, and thermonuclear resources. This book assesses the results of many years of research. Its contributors report investigations conducted on the large operating U-20 and U-25 MHD facilities and discuss problems associated with the design and construction of the world's largest commercial-scale MHD powerplant. The book also examines spatial electrodynamic problems; supersonic and subsonic, inviscid two dimensional flows; and nonideal behavior of an MHD channel on local characteristics of an MHD generator.

TO ORDER: Write AIAA Order Department,
370 L'Enfant Promenade, S.W., Washington, DC 20024

Please include postage and handling fee of $4.50 with all orders. California and D.C. residents must add 6% sales tax. All orders under $50.00 must be prepaid. All foreign orders must be prepaid. Please allow 4-6 weeks for delivery. Prices are subject to change without notice.

1986 588 pp., illus. Hardback
ISBN 0-930403-05-3
AIAA Members $49.95
Nonmembers $69.95
Order Number V-101